Time-diagnostics for improved dynamics experiments at XUV FELs

Markus Drescher, Ulrike Frühling, Maria Krikunova, Theophilos Maltezopoulos, Marek Wieland

Time-diagnostics for improved dynamics experiments at XUV FELs

Markus Drescher, Ulrike Frühling, Maria Krikunova, Theophilos Maltezopoulos, and Marek Wieland

Institut für Experimentalphysik, University of Hamburg, Luruper Chaussee 149, 22761 Hamburg, Germany

E-mail: `markus.drescher@desy.de`

Abstract. Significantly structured and fluctuating temporal profiles of pulses from SASE free electron lasers as well as their unstable timing requires time-diagnostics on a single-shot basis. The duration and structure of XUV pulses from the Free Electron Laser in Hamburg (FLASH) are becoming accessible using a variation of the streak camera principle, where photoemitted electrons are energetically streaked in the electric field component of a terahertz electromagnetic wave. The timing with respect to an independently generated laser pulse can be measured in an XUV/laser cross-correlator, based on a non-collinear superposition of both pulses on a solid state surface and detection of XUV-induced modulations of its reflectivity for visible light. Sorting of data according to the measured timing dramatically improves the temporal resolution of an experiment sampling the relaxation of transient electronic states in xenon after linear- as well as non-linear excitation with intense XUV pulses from FLASH.

1. Introduction

The new generation of linear-accelerator-based extreme-ultraviolet (XUV) and X-ray free electron lasers (FEL) represent extremely promising light sources for studying the dynamics of electronic and nuclear rearrangements in atoms, molecules, on surfaces, and in bulk material. Short wavelengths guarantee high spatial resolution in diffraction experiments [1, 2] and facilitate deep penetration of the radiation into the electron shells, thus providing chemical specificity [3]. High flux yields sensitivity down to the single-molecule level [4] and high peak intensities enable remarkable steps towards nonlinear optics in the X-ray range [5, 6]. Finally and most significantly, the short pulse duration opens the door for utilizing well-developed X-ray tools for exploring the response of matter to an optical stimulus on the relevant time-scale.

The full exploitation of this potential not only requires an optimization of these properties but also relies strongly on the capability to deal with the issue of reproducibility: It turns out, that the currently operated and commissioned FEL sources based on self-amplified spontaneous emission (SASE) are subject to pronounced shot-to-shot variations of basically all radiation properties, including pulse energy and spectrum, as well as the spatial and temporal profile. In the long-term, significant progress is expected from advanced concepts like injection seeding of the undulators [7], but on a more temporary scale much improvement can be achieved by utilizing a tagging concept. If the properties of individual FEL pulses are measured independently, the data of simultaneously performed experiments can be filtered or sorted according to these attributes. For a correction of pulse energy variations this concept is readily available to users of FLASH by virtue of an energy monitor with single-shot capability [8], after the current major shutdown also spectral measurements will be available for each FEL pulse. This article reports on recent progress in obtaining single-shot information on i) the duration / temporal profile of individual pulses from FLASH and ii) their relative timing with respect to laser pulses delivered by the facility.

In contrast to lasers in the visible range, FELs operated in the soft and hard X-ray regime are currently lacking optical resonators that would provide a selection of defined cavity modes. Instead, quantum noise is picked-up at the undulator entrance and is further amplified in the SASE avalanche [9]. As a result, an unpredictable pattern of modes is formed within the spectral window $\Delta\omega$ of the FEL bandwidth. While in mode-locked laser oscillators the pulse duration Δt_{laser} corresponds almost to the Fourier-limit given by the available spectrum, i. e. $\Delta\omega \times \Delta t_{\text{laser}} \approx 1$, pulses from SASE FELs will usually exhibit several temporal modes within an envelope dictated by the duration of the lasing part of the electron bunch. Since 2005, FLASH has been operated in a mode where the electron charge banks up within < 50 fs at the leading edge of the electron bunch [10]. On the other hand, its 0.5 eV bandwidth at 100 eV photon energy corresponds to a minimum (Fourier-limited) duration of each temporal spike of about 4 fs. Thus, depending on the number of sub-pulses and their temporal distribution the total FEL pulse length will be somewhere between $4 - 50$ fs and will fluctuate erratically

between subsequent pulses. The number of sub-pulses is expected to be small (< 5) for FLASH [10] but can reach large numbers for hard-X-ray FELs.

In time-resolved experiments using the pump-probe technique for sampling the (linear) response of a system to a pulsed optical excitation with a delayed XUV pulse, it is the envelope width σ_{FEL} that enters into the achievable time-resolution. As the result is usually composed from an average over many shots, the effective resolution is determined by the average pulse envelope $\bar{\sigma}_{\text{FEL}}$. On the other hand, the outcome of experiments probing the nonlinear response of matter to an intense XUV pulse [5], may critically depend on the distribution of energy within the pulse envelope, because the process will be dominated by the peak- rather than the average intensity. For the former case, the tagging concept will help improving time-resolution by confining the analysis to data obtained with FEL pulses below a selectable threshold of measured pulse durations. For the latter case, sorting of the data according to measured durations and pulse-structure will significantly enhance the results expressiveness.

The formation of ultra-short FEL pulses involves the synchronization of the accelerating radio frequency field with the laser-driven electron gun and a second laser delivering femtosecond pulses to the experimental end stations. Stabilization of the timing between XUV- and laser pulses to a level where the resolution of time-resolved experiments would merely be limited by the FELs pulse duration will require locking of the phase of the acceleration field to the laser pulses with a precision of $\sim 2 * 10^{-5}$ rad. XUV / laser cross-correlation experiments averaging over many shots have revealed a resolution limit of 250 fs rms [11] that can be attributed to arrival time jitter at the end-station. A single-shot metrology for the timing between XUV and laser pulses will aid in the identification and reduction of jitter sources and allows an immediate improvement of the resolution by jitter compensation.

In section 2 a technique for obtaining single-shot information on the duration of XUV pulses from FLASH will be reviewed. The instrument, a light-field driven streak camera, will be demonstrated to unveil the expected sub-structure in the temporal pulse profile, varying erratically from shot-to-shot. Section 3 reports on the single-shot determination of the FEL/laser timing, utilizing an optical cross-correlation on a solid surface in a non-collinear geometry. The improvement in temporal resolution achieved by applying the tagging concept will be reported in section 4, demonstrating a significant advance in the capability to study linear as well as non-linear electronic relaxation processes with FEL radiation.

2. Single-shot measurement of XUV pulse duration

The strongly modulated temporal profile of SASE-FEL pulses is usually also reflected in a modulation of their spectrum. Unfortunately, a straightforward measurement of the power spectrum will generally not reveal the desired temporal profile due to a lack of phase information. Streak cameras are established devices for a direct sampling of the time-profile of visible [12] as well as X-ray pulses [13, 14]. A photocathode
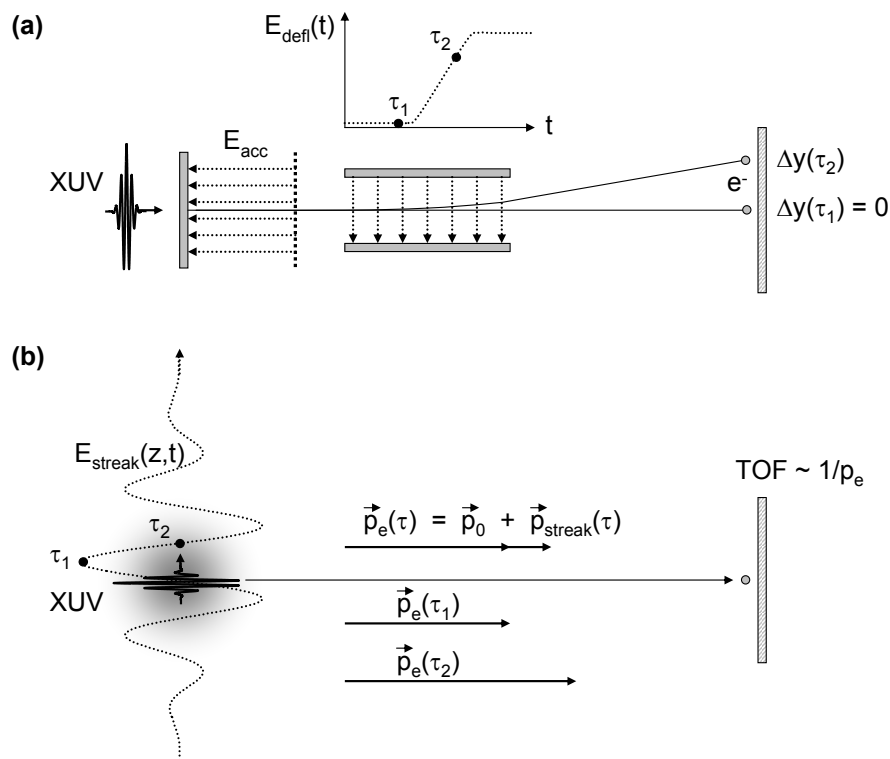
Figure 1. Schematic of streak camera principles. (a) Conventional streak camera: The XUV pulses hit a photocathode where electron bunches with temporal structures identical to those of the XUV pulses are created. The electrons are accelerated and deflected by a fast varying electrical field. The deflection depends on the time the electron enters the deflector. Thus, the temporal structure of the XUV pulses is mapped onto spatial positions of electrons on a screen. (b) Light-field driven streak camera: The XUV pulses hit a gas target, the resulting photoelectrons are accelerated by the electric field of a superimposed infrared or THz light pulse. The momentum change of the electrons depends on the state of the field at the ionisation time τ. Thus, the temporal structure of the XUV pulses is mapped onto kinetic energy modulations of photoelectrons.

transforms the incoming light pulse into an electron bunch that initially represents an exact temporal copy of the light distribution. As depicted in Figure 1(a) the electron packet is then accelerated and subsequently deflected in a transient transverse electric field. Since the transverse momentum an electron gains depends on the strength of the field at the deflector entrance, the temporal information is projected onto a spatial position on a fluorescence screen. Main factors limiting the temporal resolution of these devices are the finite rise time of electro-optical switches creating the transient field and the spread of the propagating particle wave packet introduced by Coulomb repulsion and dispersion. These constraints are removed by utilizing a variant of the streak camera principle, where the solid photocathode is substituted by an atomic gas and the deflecting field slope is replaced by the electric component of an oscillating electromagnetic field (Figure 1(b)). Much higher temporal gradients of the streaking

field boost the resolution together with an elimination of the dispersive wave packet spread. As the photoemitting atoms are embedded into the streaking field, the electron wave is instantaneously sampled during its formation, thus prohibiting a temporal broadening. In contrast to a conventional streak camera, no directed electron beam is formed, but the electrons initially escape from the photoemitter in all directions according to a partial wave composition determined by the initial state and the photon energy and polarization of the ionizing radiation. Correspondingly, the streaking action of the electric field is not observed as a steering of a particular electron trajectory but rather in the form of a momentum transfer in the field direction. Thus, for this light-field streak camera the temporal information is projected onto a change of the detected kinetic electron energy. The time-resolution achievable with this type of instrument is ultimately limited only by the speed of the photoemission process [15] and is therefore used in attosecond physics for the characterization of XUV photon pulses with durations of about 100 as [16, 17]. In those studies a near-infrared field with an oscillation period of only ~ 2.5 fs (800 nm wavelength) was employed. Even at moderate laser intensities the rapid change of the streak field guaranteed an extreme streaking speed above 10 eV/fs. It is determined by the rate of change of the electron kinetic energy with the delay between photon pulse and streaking field. For the characterization of FEL pulses with an expected duration of up to 50 fs the streaking electromagnetic radiation must obey a monotonically rising electric field within this interval. This implies a lower wavelength-limit of 30 μm, i.e. radiation in the terahertz (THz) regime. Targeting a streaking field induced energy shift ΔW of twice the spectral width σ_W of the photolines requires a field strength E_streak according to

$$\Delta W = e\, E_\text{streak}\, \lambda_\text{streak} \sqrt{\frac{W_0}{2\pi^2 m_e c^2}} > 2\,\sigma_\text{W} \qquad (1)$$

with the initial kinetic electron energy $W_0 = \text{IP} - h\nu_\text{x}$, given by the ionisation potential IP of the atomic medium at the photon energy $h\nu_\text{x}$, and with e and $m_e c^2$ the electron charge and rest energy, respectively [23]. For $W_0 = 100$ eV, $\sigma_\text{W} = 1$ eV, and a wavelength $\lambda_\text{streak} = 100$ μm for example, the electric field strength shall exceed 6 MV/m. Note that the scaling with λ_streak reduces the required light intensities $I \approx E^2$ by many orders of magnitude upon changing streaking wavelengths from the near-infrared to the far-infrared (= THz) regime.

In the THz field driven streak camera experiment at FLASH 13.5 nm pulses are collinearly overlapped with intense linearly polarised THz-pulses from the FLASH THz undulator [18, 19] in a gas target (krypton or xenon). The gas atoms are ionised by the XUV pulses. The kinetic energies of the resulting photoelectrons are measured with two time-of-flight (TOF) spectrometers, one parallel and one perpendicular to the THz-polarisation plane. The photoelectrons are accelerated by the THz field in the direction of its polarization, thereby the temporal structure of the XUV pulses is mapped onto changes of kinetic energies of photoelectrons with a final drift velocity parallel to the THz polarization. On the other hand, the THz-field-induced energy shift of photoelectrons with a final drift velocity perpendicular to the THz polarization is

negligible (since $U_P << W_0$) and their energy distribution represents the spectrum of the XUV pulses shifted by the binding energy of the electrons. Thus, it is possible to measure simultaneously the streaked photoelectron spectra and the XUV spectra with the two electron spectrometers. For details of the setup see [20].

2.1. Mapping of the THz-field

For a measurement of the XUV pulse duration by THz streaking a precise knowledge of the time-dependent streaking field is essential. It can be sampled by measuring the field induced energy shift of the photoelectrons upon scanning the time delay between the THz and XUV pulses. The energy shift directly represents the vector potential

$$A_{\text{THz}}(t) = \int_t^\infty E_{\text{THz}}(t')dt' \tag{2}$$

of the THz pulse [21], where E_{THz} is the THz electric field. Figure 2 shows a series of kinetic energy spectra of Xe 5p photoelectrons detached by 13.5 nm FLASH pulses in the presence of intense THz pulses. The delay between both pulses was varied in steps of 33 fs and each spectrum represents an average over 25 shots. The spectra in Figure 2(a) were measured without any THz filters. The ten oscillations of the field correspond to the ten periods of the THz undulator [22]. A Fourier transformation of the THz vector potential yields the THz spectrum consisting mainly of the fundamental at 92 μm with a bandwidth of 10% and small contributions of the second and third harmonic which is consistent with simulations [22] and spectral measurements.

For the measurement of the XUV pulse duration a smooth THz field is essential. Therefore, a THz bandpass filter (QMC Instruments) transmitting between 82 and 107 μm was used during these measurements. This way the spectral content of higher harmonics is removed and the field is smoothened (Figure 2(b)). From the observed oscillation a wave period of 306 fs can be extracted. This corresponds to a wavelength of 92 μm and a frequency of 3.3 THz. The maximal field strength was 50 MV/m and the maximal streaking speed was typically in the order of 0.1 eV/fs. At the FLASH facility, the same electron bunches are used to produce both the XUV and the THz pulses, therefore a good synchronization of the pulses is expected. If the delay between the XUV and THz pulses is set close to a zero transition of the THz vector potential a small timing jitter between both pulses translates into energy fluctuations of the streaked photoelectrons. By analyzing the fluctuation of the mean energy of single-shot photoelectron spectra measured with and without the THz pulses, respectively, a jitter of 5 fs root mean square (rms) was determined.

### 2.2. Measurement of the XUV pulse properties

To determine the duration and the linear chirp of the FLASH XUV pulses the delay between the XUV and THz pulses was set to zero transitions of the THz vector potential and streaked and non-streaked single shot photoelectron spectra were measured simultaneously. The applied streaking field leads to a time dependent energy
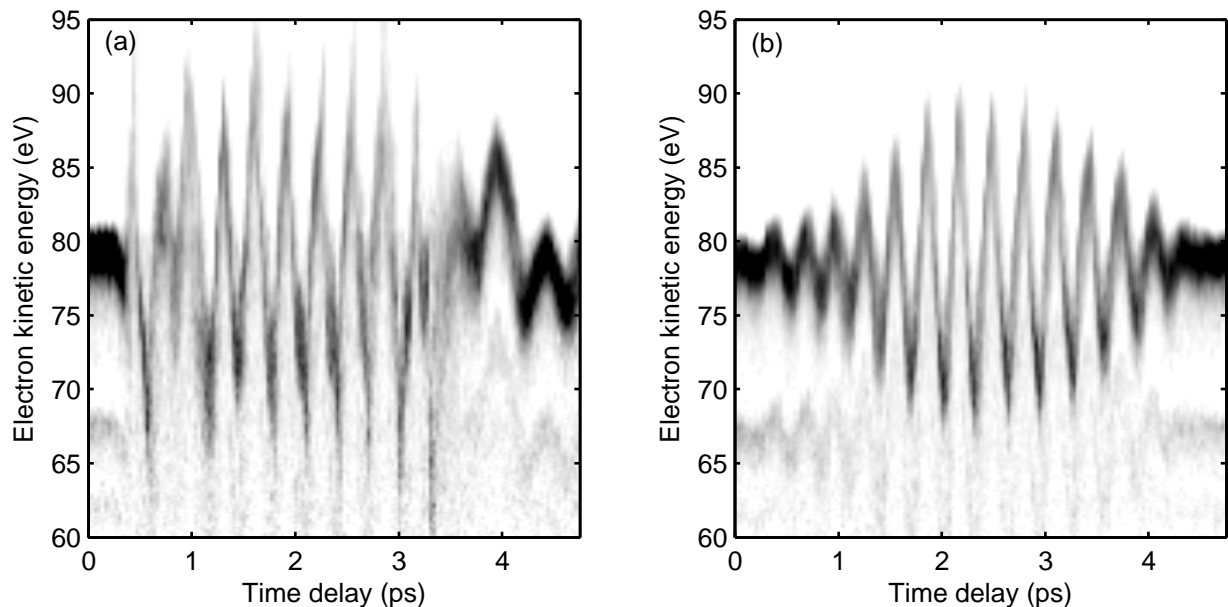
Figure 2. Sampled THz vector potential. Series of kinetic energy spectra of 5p electrons detached from xenon atoms by a 13.5 nm XUV pulse in the presence of an intense pulsed THz field. The energy shift of the electrons versus the XUV/THz delay directly represents the vector potential A_{THz}. The less intense electron signal at lower energies stems from stronger bound xenon 5s electrons. The spectra shown in (a) were measured without any THz filters. For the measurement of the spectra in (b) a bandpass filter was used to narrow and smooth the THz spectrum.

shift of the electron wave packet, with a sign depending on the sign of the slope of A_{THz}. If the XUV pulse carries a linear frequency chirp, the resulting total chirp and thus the width of the streaked spectra is enlarged or reduced for consecutive zero transitions of A_{THz} respectively [23]. Based on such analysis, the chirp of attosecond XUV pulses has previously been determined [24]. Under the assumption of a Gaussian pulse shape and a constant linear chirp the pulse durations of the individual XUV pulses were deduced (Figure 3). The average pulse duration was 35 fs FWHM with a width of the distribution (standard deviation) of 9 fs. A small percentage of the pulses has pulse durations of less than 7 fs FWHM.

The employed gas target does not significantly alter the XUV pulses, so it is possible to measure the XUV pulse duration simultaneously to other time-resolved experiments. By sorting the measured data according to the XUV pulse duration a significant increase of the temporal resolution of XUV-pump/X-ray-probe experiments can be expected. For a fast reconstruction of the pulse duration of many shots a Gaussian pulse shape was assumed. In addition, for some pulses it is possible not only to reconstruct the pulse duration or envelope of the pulse but also a temporal sub-structure consisting of separated spikes. Figure 4 shows an example of a streak spectrum with two clearly resolved peaks (b) and the corresponding non-streaked photoelectron spectrum (a). To reconstruct the temporal structure of the XUV pulse two Gaussian sub-pulses were
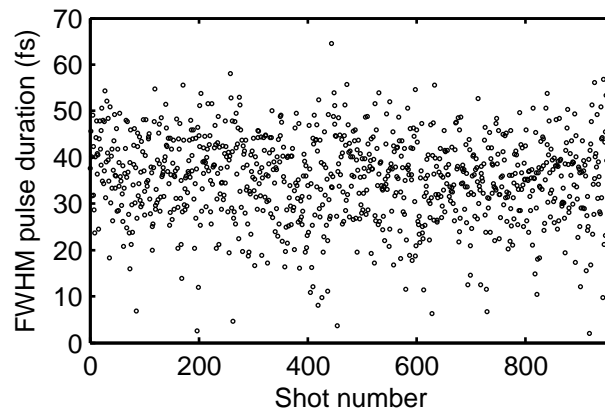
Figure 3. Reconstructed pulse durations. FWHM durations of 960 consecutive 13.5 nm FLASH pulses reconstructed by an analysis considering a Gaussian pulse profile.
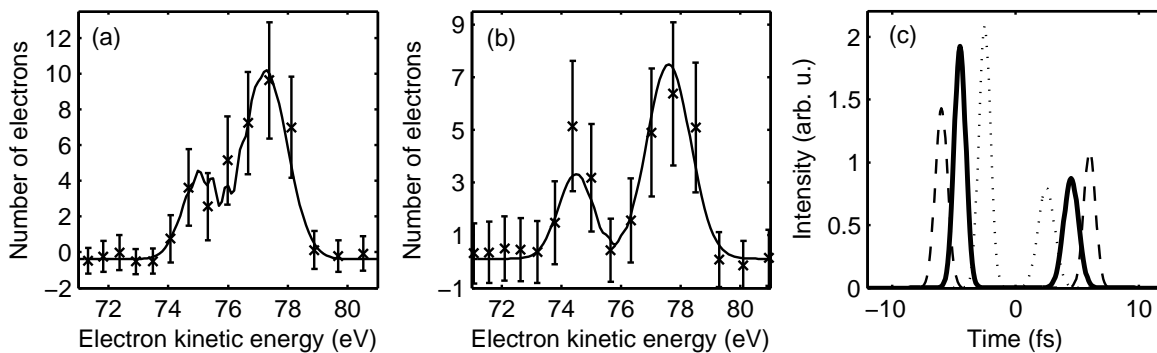
Figure 4. Single-shot photoelectron spectra and reconstructed temporal structure. Non-streaked (a) and streaked (b) photoelectron spectra of a single FLASH XUV pulses. The vertical bars indicate the statistical error given by the number of electrons detected within a 0.7 eV-wide kinetic energy bin. Plotted as lines are simulated spectra that best fit the measured ones. The bold line in (c) is the reconstructed temporal structure that best fits the measured spectra. The dashed and dotted lines correspond to the upper and lower limit of the 90% confidence region for the delay. (adapted from [20])

assumed and the corresponding streaked and non-streaked spectra were calculated. The central energies, amplitudes, widths and the temporal separation of the sub-pulses were optimized to fit the measured spectra. The optimized spectra are plotted as lines in Figure 4. The corresponding temporal structure is plotted as a bold line in Figure 4(c). For the analyzed spectra about 10% showed two or more well separated features, whereas 90% had a compact envelope.

3. Single-shot measurement of Laser / XUV timing

3.1. Concepts of XUV / laser cross-correlation measurements

Since in a single-shot instrument a scan of the delay between both pulses in subsequent shots is not possible, the timing information must be encoded in a measurable parameter. Spatial encoding utilized here requires the superposition of both beams on the target under a certain angle. This way, the pulse-fronts intersect each other at different locations with different relative timing, thus mapping the temporal delay onto a spatial coordinate.

Arrival time fluctuations of the XUV pulses from FLASH relative to the laser pulses were measured with two different cross-correlation techniques at the experimental end-station. Any cross-correlation between two light waves relies on the mediation by a target that delivers an observable which depends simultaneously on both radiation fields. The XUV and laser pulses were non-collinearly superimposed in space and time in a noble gas target and on a solid surface, respectively. For the noble gas cross-correlator the observable is the electron sideband formation, where the XUV generated photoelectrons are shifted to spectral sidebands by the laser field [25]. For the solid surface cross-correlator the observable is a reflectivity modulation of the surface. Here the illumination of the surface with XUV pulses from FLASH significantly changes the crystal's reflectivity for laser light [26].

The experimental setup of the cross-correlator using sideband formation is shown in Figure 5(a). The unfocused XUV pulse enters the target chamber through an entrance slit of 0.5 mm height and 0.15 mm width. In this time-to-space mapping geometry, the XUV pulse height of 0.5 mm corresponds to a time window of 1.7 ps. A krypton gas target for the generation of photoelectrons by the XUV beam is supplied by a gas nozzle. The laser pulse is focused perpendicularly to the FEL in front of the entrance aperture of the electron optical system to achieve intensities of $\sim 10^{13}$ W/cm^2 required for the formation of the spectral sidebands. Both beams are linearly polarised parallel to the axis of the electron optics and both pulses are overlapped in the interaction region in space and time. Photoelectrons from this region are energetically shifted to spectral sidebands due to the interaction with the laser light field [25]. The photoelectron energy spectrum is separated from the unperturbed photoline by multiple integers of the laser photon energy. Time-to-space mapping in this setup is achieved by imaging the interaction region with an electron lens system onto a MCP/phosphor assembly. A grid in the electron path realizes a high-pass energy filter, which separates the energetically up-shifted sideband electrons from the unperturbed photoelectrons by applying a retarding voltage. A detailed description of this experiment can be found in [27].

The experimental setup of the cross-correlator on a solid surface is shown in Figure 5(b). Here, the unfocused and spatially filtered laser pulse illuminates the entire area of a GaAs or Si_3N_4 sample and the reflected light is imaged with a lens system onto a CCD camera. The horizontally propagating focused XUV pulse is absorbed in
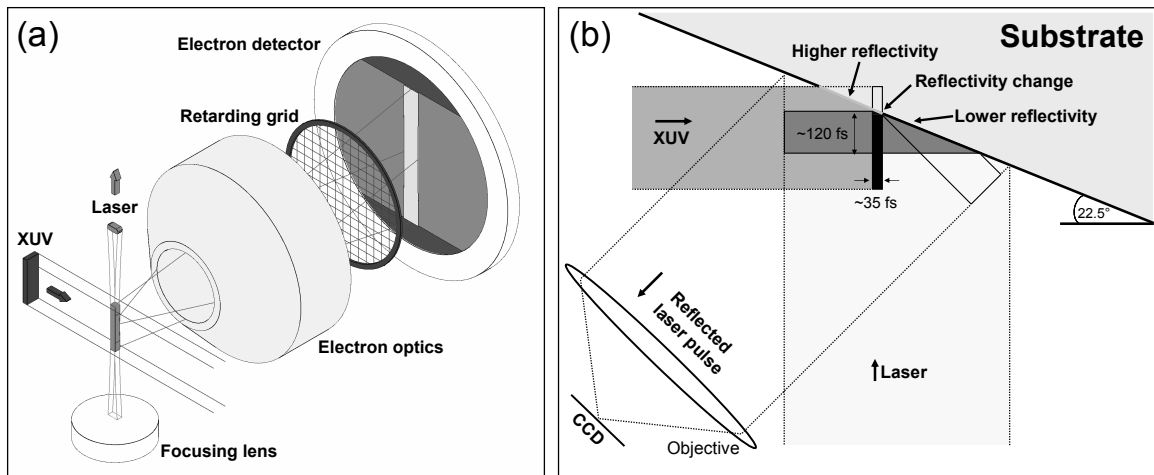
Figure 5. Different cross-correlation schemes (a) Unfocused XUV and focussed laser pulses are superimposed in a krypton gas target. The electrons in spectral sidebands from the region of temporal and spatial overlap are imaged by an electron lens system with a high-pass energy filter. (b) An unfocussed laser pulse is reflected from a solid substrate onto a CCD camera. The focused XUV pulse is absorbed in the substrate and changes the reflectivity for the laser pulse. The boundary of reflectivity change is used as arrival-time marker for the XUV pulse.

the sample, creating a highly excited electron distribution with significantly changed optical properties for the laser pulse. The sign of a resulting change in reflectivity for visible light depends on the choice of material and was found to be negative for GaAs at ~ 44 eV exciting photon energy and positive for Si_3N_4 at ~ 90 eV. In the chosen non-collinear geometry, the spatial position of the reflectivity change is a direct measure for the relative delay between XUV and laser pulse, again mapping time- into space-information. A detailed description of this experiment can be found in [28] and [29].

3.2. Cross-correlation based on sideband signal from rare gas photoionization

The cross-correlation signal of photoelectrons in krypton excited by 32 nm radiation is shown in Figure 6. In (a) an electron optical image obtained at temporal overlap after summation over several macro pulses is presented. The photoelectrons from spatial and temporal overlap, which are spectrally up-shifted and form spectral sidebands, are separated from the main photo line with the high-pass energy filter. It should be noted, however, that the signal of a single shot image is far too low. In order to get an evaluable image it requires a summation over many individual pulses. A delay scan reveals additional signal from these electrons at distinct delay settings, which is shown in Figure 6(b). Every data point corresponds to one macro pulse containing 30 micro pulses. The Gaussian fit shows a temporal width of 1.9 ps FWHM. This value is the result of a convolution between the experimental temporal window (1.7 ps), the jitter (~ 1 ps), and the pulse widths of the XUV (35 fs) and laser pulses (120 fs). The
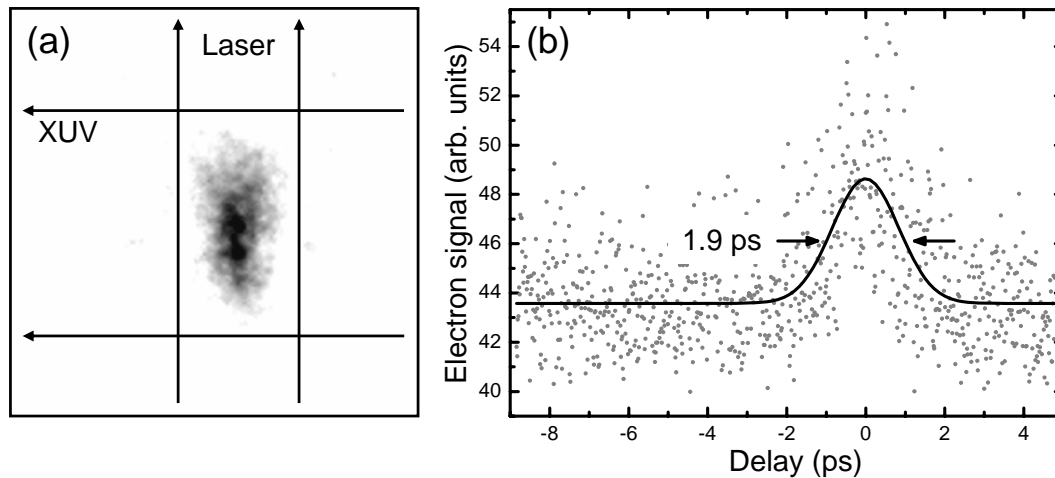
Figure 6. **Averaged electron cross-correlation signal in a krypton gas target** (a) Sideband-photoelectron image at temporal overlap (fixed delay). XUV and laser paths are marked with arrows. The image is generated by summation over 1200 macropulses with 30 micropulses and is background subtracted. (b) Integrated sideband-photoelectron signal plotted as a function of XUV/laser delay. Spectral sideband signal appears only at temporal overlap of both pulses. Every data point corresponds to one macropulse with 30 micropulses. .

comparably high jitter value results from the machine performance in the beginning of the user operation of FLASH. Meanwhile, significant progress has been achieved in short and long term timing stability (see Figure 8). While this set-up in principle facilitates single-shot XUV arrival time measurements, the present signal level requires averaging over many pulses in order to obtain sufficient signal.

An enhancement of the sideband signal can be achieved by either increasing XUV pulse energy or laser intensity in the interaction region. However, no electron image formation could be achieved with increased XUV pulse energies due to space charge effects. So far, only 0.015 mJ laser pulses could be applied with this technique. Meanwhile, laser pulses with 2 mJ pulse energy are available at the experimental end-station of FLASH. With two orders of magnitude stronger laser intensities a more efficient sideband formation could enable single-shot data acquisition with this technique in the future.

3.3. Single-shot arrival time measurements using the solid surface cross-correlation

Image distorting space charge effects are completely avoided in the photon-in / photon-out cross-correlation set-up sketched in Figure 5(b). A typical image of a single-shot cross-correlation using a Si_3N_4 substrate is shown in Figure 7(a). The area, where the XUV pulse (13 nm) has excited the Si_3N_4 sample prior to the arrival of the laser pulse, appears brighter. An average of horizontal signal pixels within the region of interest (ROI) marked in Figure 7(a) is shown in (b). One pixel on the CCD chip corresponds to a 17 fs step of the XUV relative arrival time. The rising edge of the signal is in the range
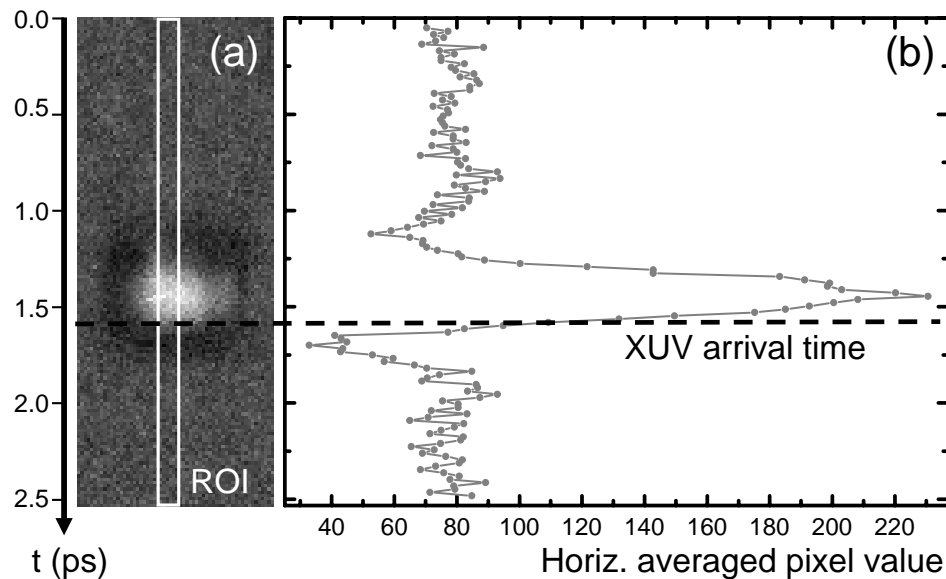
Figure 7. Single-shot arrival time measurement by reflectivity change on Si_3N_4 (a) Areas where the XUV pulse hits the substrate before the laser pulse is reflected appear brighter. For the time axis t (shown on the left) the zero point is set arbitrarily to the top of the image. (b) Horizontally average signal of pixels within the ROI marked in (a). One pixel corresponds to 17 fs. The inflection point marked as dashed line is used as an XUV arrival-time marker.

of the laser pulse duration (120 fs). The inflection point (marked as dashed line) is used as arrival-time marker for the XUV pulse. The developed timing tool can be operated with a fraction of the XUV fluence delivered by FLASH, needs very little energy from the laser pulse and does not require sample-scanning since the underlying physical process is completely reversible. In this manner, the XUV arrival-time is measured directly at the experimental end-station and, thus, takes all possible jitter sources into account. Figure 8(a) shows a sequence of 18 single-shot cross-correlation images. Due to arrival-time fluctuations of the XUV pulses, the region of reflectivity change fluctuates from shot-to-shot. A histogramm of arrival times, which are deduced out of 515 single-shot images, is plotted in Figure 8(b). The Gaussian fit shows a FWHM of 408 fs. Thus, without corrections a multi-shot pump-probe experiment using XUV and laser pulses will be limited to this temporal resolution. The single-shot arrival-time measurement demonstrated here is a way to improve the temporal resolution by sorting the pump-probe spectra pulse-by-pulse according to the measured delay as will be demonstrated in the next chapter.

4. Jitter-compensated pump-probe experiments

In the previous section the XUV/laser cross-correlator for the single-shot arrival time measurement of FLASH pulses was introduced. In the following the improvement obtained by the simultaneous operation of the cross-correlator with a XUV pump/visible
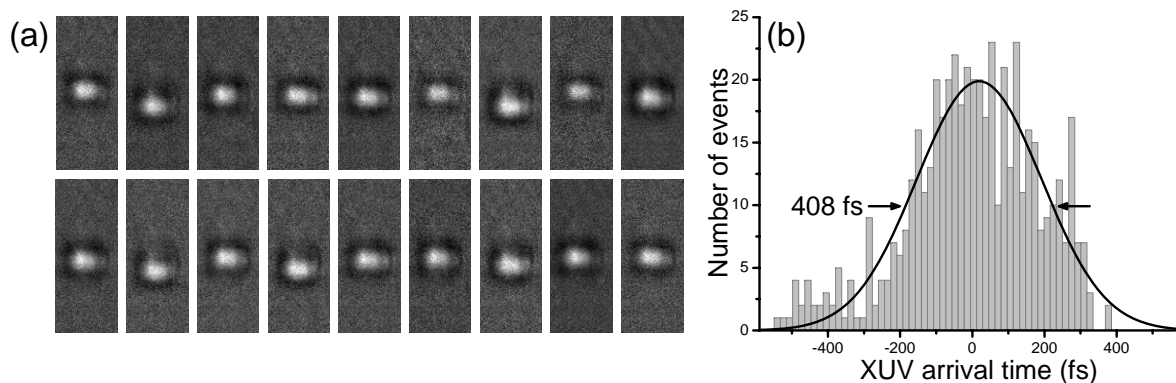
Figure 8. Series of XUV/laser single-shot cross-correlation images (a) XUV arrival times with respect to the laser for 18 arbitrarily chosen single-shots. (b) Arrival time distribution for the complete data-set of 515 shots with 17 fs binning.

probe experiment is demonstrated. For the first proof-of-principle, ion-charge-state spectrometry for studies of the time-resolved electron dynamics was selected [29]. In this approach, an inner-shell vacancy created in an atom by the XUV (pump) pulse decays preferably via radiation-less electron relaxation resulting in the ejection of one or more (Auger) electrons. Depending on the intermediate states involved in the de-excitation process several multiple-charged ionic states are created. The population of the intermediate excited ionic states is probed with a delayed optical laser pulse via multi-photon ionisation (or tunneling). Different ionic states created in the target volume are detected by a time-of-flight (TOF) ion mass-to-charge spectrometer by changing the time delay between pump and probe pulses. From the shape of the transient ion yield the lifetime of excited states can be extracted.

An implementation of ion-charge-state spectrometry at intense photon-sources like FLASH has several advantages compared to photo-electron spectroscopy. Ions are less sensitive to space charge effects than electrons making the measurements feasible at much higher XUV fluence. Furthermore, the ion yield is less influenced by the spectral fluctuation of FEL pulses than the kinetic energy distribution of the photo-lines. Combined with a high detection probability ion-charge-state spectrometry allows single-shot data analysis. The shape of the transient pump-probe signal is generally described by the convolution integral over a response from the sample and an instrument response function. The sample response is defined by the lifetime of the intermediate excited states involved. The instrument response determines the experimental time resolution and can be approximated by a Gaussian with a FWHM Δt:

$$\Delta t = \sqrt{\Delta t_{\text{laser}}^2 + \Delta t_{\text{XUV}}^2 + \Delta t_{\text{jitter}}^2}, \tag{3}$$

Thus, selecting the system with well known dynamics as a reference the experimental time resolution can be extracted from the data. Currently, the pulse duration $\Delta t_{\text{laser}} = 120$ fs (FWHM) of the optical laser system provided by the FLASH user facility dominates against the much shorter XUV pulses $\Delta t_{\text{XUV}} = 35$ fs (FWHM). A substantial
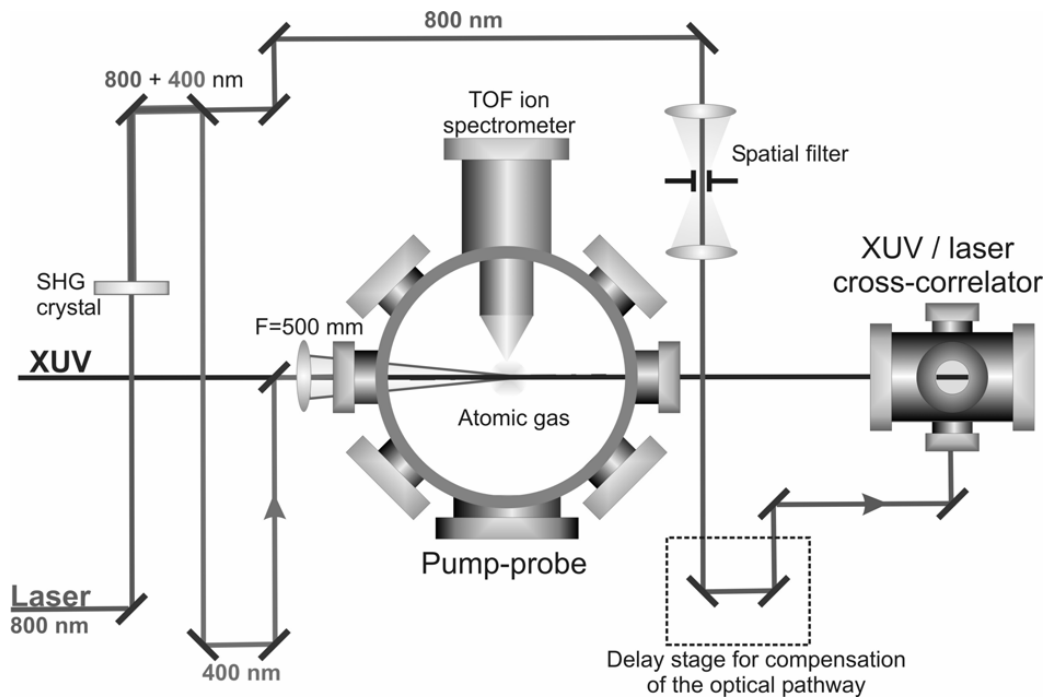
Figure 9. Scheme of the experimental geometry (top view) Pump-probe experiment installed before the XUV/laser cross-correlator setup shares the same XUV beam. The 800 nm optical laser pulses are frequency doubled and overlapped at a small angle in a Xe gas target of the pump-probe experiment. A TOF ion mass-to-charge spectrometer detects ions created in the interaction region. The cross-correlator is operated with the remaining spatial frequency filtered 800 nm light. A delay stage before the setup compensates for the optical pathway difference between both experiments.

arrival time jitter Δt_{jitter} of the XUV pulses with respect to an external laser will further diminish a temporal resolution.

4.1. Exploring the intrinsic temporal resolution of FLASH with the time-resolved ion-charge-state spectrometry on xenon

A scheme of the experimental geometry with the pump-probe vacuum chamber installed in front of the cross-correlator setup is shown in Figure 9. An optical delay line available at FLASH scans the arrival time of the optical laser with respect to the XUV pulse from negative values (optical probe first) to positive values (XUV pump first) within a several ns time window. Another delay stage introduced before the cross-correlator setup compensates for the optical pathway difference between both experiments. The delay time zero corresponds to the coincidence of the peaks of the XUV and laser pulses and is determined subsequently from fitting to the experimental data (see [29] for details).

As a reference for an assessment of the achieved jitter compensation a relaxation
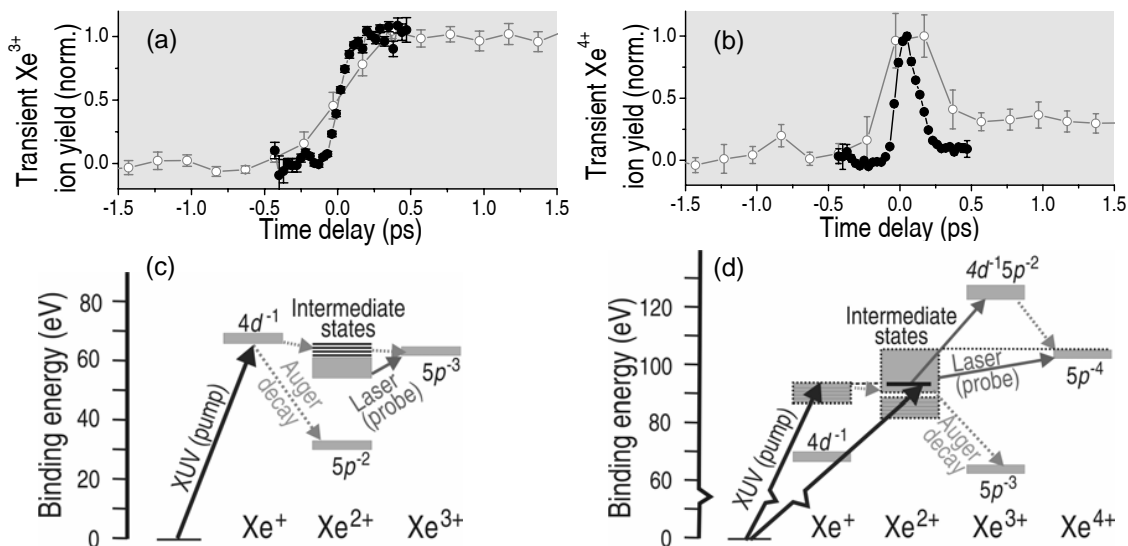
Figure 10. (a) Transient Xe^{3+} and (b) Xe^{4+} ion yields, background subtracted and normalized, as a function of the time delay between XUV pump and visible probe pulses. Gray open circles denote a delay scan without correction of the XUV pulse jitter. The time window of transient changes in the ion yield is noticeably contracted as a result of jitter compensation with the XUV/visible cross-correlator (black circles). (c) and (d) are transitions in Xe, excited by XUV and probed by visible laser pulses, responsible for transient Xe^{3+} and (b) Xe^{4+} ion yields, respectively.

process in xenon atoms following a $4d$ core excitation within the $4d \rightarrow \epsilon f$ giant resonance was selected. The relaxation pathways of the created vacancy via single (A1) and double (A2) Auger decay involving several intermediate states were directly observed by detecting $4d$ and two Auger electrons in coincidence [30]. Time constants for the Auger decay of $\tau_{A1} = 6.0 \pm 0.7$ fs and $\tau_{A2} = 30.8 \pm 1.4$ fs leading to Xe^{2+} and Xe^{3+} final states with two or three vacancies in the outer $5p$ shell, respectively, are known with high precision from time-domain studies [31] and energy-resolved measurements [32]. Averaged Xe^{3+} and Xe^{4+} ion yields (grey opened circles) as a function of the time delay are plotted in Figure 10(a) and (b) together with a simplified scheme of energy levels and transitions (c) and (d). The data set was collected by scanning an optical delay line with 10 second acquisition time (50 shots) per 200 fs step, without any compensation for the XUV arrival time jitter. The shape of the transient Xe^{3+} and Xe^{4+} profiles manifests the fast rising edge characterized by the lifetime of the $4d$ hole (τ_{A1}). The laser-enhanced Xe^{3+} ion yield shows no decrease for positive delays in correspondence with a long life time of the intermediate states as compared to the experimental time scale (Figure 10(c) and [31]). The electron dynamics leading to the transient Xe^{4+} ion yield is governed by short-lived intermediate excited states (Figure 10(d) and τ_{A2} in [31]) leading to a fast decrease for positive time delays. Transient changes of the ion yields are observed within a noticeably broad time window (Figure 10(a) and (b)). The extracted time resolution $\Delta t \approx 450$ fs is clearly dominated by the XUV arrival

time jitter Δt_{jitter} estimated from the histogram of XUV arrival times measured with the XUV/laser cross-correlator (Figure 8(b)).

Within a second run (black closed circles in Figure 10(a) and (b)) the data set was collected at a fixed delay stage position and simultaneously tagged with XUV arrival time information from the XUV/laser cross-correlator. The data were accordingly arranged in 30 fs time bins. The time window of the observed transient changes in the Xe^{3+} and Xe^{4+} ion yields is considerably contracted (Figure 10(a) and (b)), demonstrating a substantial improvement in the temporal resolution of the transient signal. The degree of improvement is further corroborated by the extracted time resolution $\Delta t = 125 \pm 5$ fs (standard deviation) in good correspondence with the expected 125 fs by assuming a complete compensation of the arrival time jitter Δt_{jitter}. The established temporal resolution is now dominated by the optical laser pulse duration. Using shorter laser pulses the precision of the introduced tagging technique carries the potential of pushing the temporal resolution towards the intrinsic limit dictated by the XUV pulse duration.

4.2. Multi-parameter data tagging revealing nonlinear dynamics of the XUV-excited Xe $4d^{-2}$ core holes

The power of the introduced data tagging approach is especially underlined by the observation of a new electron relaxation pathway manifested in the Xe^{5+} transient ion yield. The threshold for the Xe^{5+} formation is about 168 eV, i.e. significantly higher than the 92 eV exciting photon energy. Based on the nonlinear behaviour of this previously not observed decay channel it was attributed to a double photo-ionisation of the $4d$ core electron shell [29]. Figure 11 shows energy levels and transitions involved in the formation of the transient Xe^{5+} ion yield. A double ionisation of the $4d$ shell by a two-photon absorption leads to a $4d^{-2} \rightarrow 5p^{-4}$ decay, while additional energy introduced by an intense laser pulse activates a $4d^{-2}5p^{-1} \rightarrow 5p^{-5}$ channel. The results indicate a particular role of the $4d \rightarrow \epsilon f$ giant resonance in increasing the double ionisation probability in Xe compared to other rare gases in accordance with [33]. An observation of multi-photon processes is generally hampered by high intensity fluctuations. Figure 11(b) demonstrates the sensitivity of the Xe^{5+} ion yield to the XUV pulse energy. No time dependence of the Xe^{5+} signal (grey closed circles) can be resolved below 1 μJ of XUV pulse energy. The relatively low statistics at negative time delays is explained by the difficulty to determine an inflection point at the top of the time window of the cross-correlator at low XUV fluencies. Black open circles in Figure 11 are filtered from the same experimental run according to the XUV intensities higher than 3 μJ. Transient changes in the Xe^{5+} ion yield similar to the Xe^{4+} ion yield are now clearly resolved.
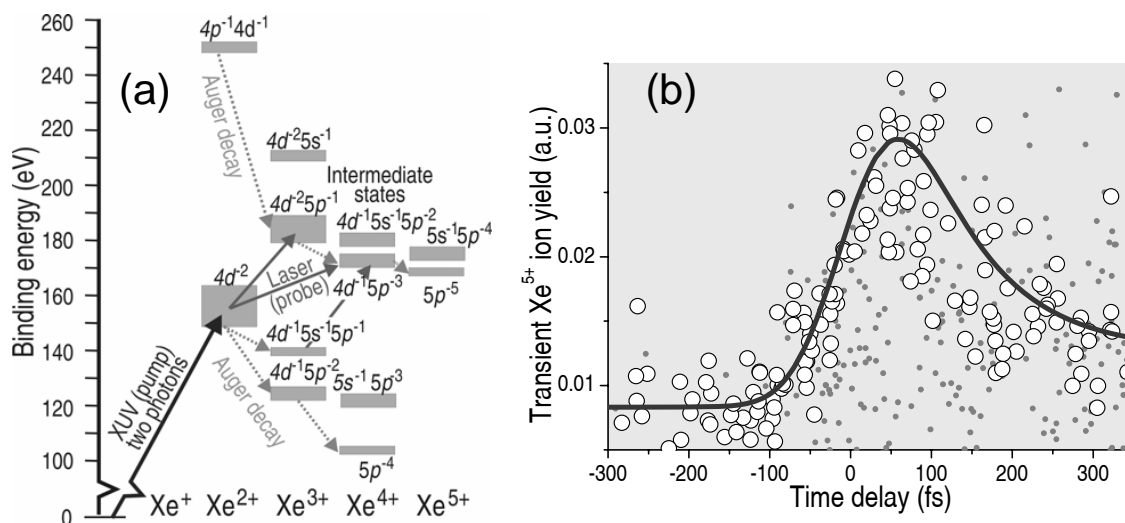
Figure 11. (a) Transitions in Xe excited by XUV pulses (adopted from [34]) and probed by visible laser leading to a transient formation of Xe^{5+} signal. (b) Single-shot Xe^{5+} ion yield as a function of the time delay: Data (open circles) measured at XUV energies higher than 3 μJ with corresponding fit (solid line) and data obtained at pulse energies below 1 μJ (closed circles). The ion yield was scaled in order to superimpose both data sets. Data are tagged according to the XUV arrival time measured by the XUV/laser cross-correlator.

5. Summary and Conclusion

Tagging proves to be a powerful concept for dealing with the intrinsically unstable character of XUV or X-ray pulses from FELs operated in a SASE mode. For the particularly demanding measurement of the temporal properties of individual pulses, solutions have now been found, where the time-information, being inaccessible to even the fastest direct detectors, is encoded in a spectral or spatial coordinate, respectively, thus making it available to slow detection schemes.

A light-field streak-camera, driven by a strong electromagnetic THz field demonstrates a temporal resolution better than 10 fs, significantly beyond the capabilities of conventional X-ray streak cameras. The deduced mean duration of (35 ± 9) fs coincides well with the value of (29 ± 5) fs obtained with an XUV/XUV autocorrelation, which has successfully been demonstrated at FLASH in an averaging mode [35]. In addition to the single-shot capability, as a matter of principle the THz/XUV cross-correlation mechanism can yield more detailed information than an autocorrelation. The streaking data allow an extraction of spectral phase information to an extent that is determined by the number of simultaneously acquired non-redundant samples of a single streaking event and the associated signal-to-noise-ratio. In the current implementation, observation in two orthogonal directions suffices to asses the complexity of a pulse, to allocate a temporal width to the ones with a compact shape, and to resolve the sub-structure of pulses with a low complexity.

The jitter issue between XUV pulses from FLASH and external laser pulses has been successfully attacked by realization of a single-shot XUV/laser cross-correlator. Compared to a temporal correlation between the laser and the accelerated electron bunch [36], the optical/optical cross-correlation removes jitter sources associated with the SASE process itself and the transport of the laser beam to the experimental endstation. A direct comparison [29] suggests that the all-optical method yields superior results if a resolution below 100 fs is desired. The degree of improvement obtained by removing jitter upon tagging individual pulses with measured delays was tested in XUV-pump/laser-probe experiments on an atomic sample. A remarkable reduction of the rise time of averaged data from ~ 400 fs to ~ 100 fs could be demonstrated. This figure is currently limited by the laser pulse duration; as soon as shorter laser pulses become available further advance is to be expected to a level where the temporal resolution approaches the XUV pulse duration and the information of the time structure of each FLASH pulse extracted from the single-shot THz-field-driven X-ray streak camera will become important.

So far the methods discussed in this article, have been tested using pulses in the soft-X-ray range below 100 eV photon energy. Extension to harder X-rays is straightforward in the case of THz streaking. As the streaking amplitude ΔW scales with $\sqrt{W_0}$ (Equation 1) and the FEL bandwidth σ_W with W_0, their ratio $\Delta W/\sigma_W$ scales with $1/\sqrt{W_0}$. For preserving contrast the streaking field strength E_{THz} must be increased according to $\sqrt{W_0}$, i.e. the square root of the photon energy. This weak scaling should facilitate the analysis of single X-ray pulses extending well into the keV range. An assessment of the scalability of jitter compensation towards harder radiation is more demanding because it relies on the specific properties of the used surface material and on the corresponding physical processes evolving after excitation with X-rays. As a general rule, the material should be chosen to contain elements that exhibit reasonable absorption at the desired wavelength, i.e. above an absorption edge.

Combining the now available techniques for the characterization of varying temporal, spectral, energetic, and spatial properties of individual X-ray pulses from SASE FELs many of the constraints connected with those fluctuations can be removed or relaxed. Still, as studies of nonlinear processes or more generally of dynamics that depends critically on the evolution of the instantaneous intensity, spectrum, and phase will require the optimal definition of the exciting radiation, this passive approach cannot replace further efforts to actively improve the control over the pulsed radiation delivered by linear-accelerator-based X-ray sources.

Acknowledgments

References

[1] Chapman H N et al. 2006 Femtosecond diffractive imaging with a soft-X-ray free-electron laser *Nature Phys.* **2** 839 - 843

[2] Gutt C et al. 2009 Resonant magnetic scattering with soft x-ray pulses from a free-electron laser operating at 1.59 nm *Phys Rev B* **79** 212406

[3] Bressler Ch and Chergui M 2004 Ultrafast X-ray Absorption Spectroscopy" *Chem. Rev.* **104** 1781

[4] Neutze R, Wouts R, van der Spoel D, Weckert E and Hajdu J 2006 Potential for biomolecular imaging with femtosecond X-ray pulses *Nature Phys.* **206** 752

[5] Sorokin A A, Bobashev S V, Feigl T, Tiedtke K, Wabnitz H and Richter M 2007 Photoelectric effect at ultrahigh intensities *Phys. Rev. Lett* **99** 213002

[6] Nagler B et al., 2009 Turning solid aluminium transparent by intense soft X-ray photoionisation, *Nature Phys.* **5** 693

[7] Garzella D, Harac T, Carre B, Salieres P, Shintake T, Kitamurac H and Couprie M E 2004 Using VUV high-order harmonics generated in gas as a seed for single pass FEL *Nucl. Instr. Meth. A* **528** 502-505

[8] Richter M et al. 2003 Measurement of gigawatt radiation pulses from a vacuum and extreme ultraviolet free-electron laser *Appl. Phys. Lett* **83(14)** 2970

[9] Dohlus M, Rossbach J and Schmüser P 2008 Ultraviolet and Soft X-Ray Free-Electron Lasers: Introduction to Physical Principles, Experimental Results, Technological Challenges, Springer, Berlin

[10] Ackermann W et al 2007 Operation of a free-electron laser from the extreme ultraviolet to the water window *Nature Phot.* **1** 336

[11] Radcliffe P et al. 2007 Single-shot characterization of independent femtosecond extreme ultraviolet free electron and infrared laser pulses *Appl. Phys. Lett.* **90**, 131108

[12] Breadley D J, Liddy B, Sleat W E 1970 Direct linear measurement of ultrashort light pulses with a picosecond streak camera *Opt. Comm.* **2** 391-395

[13] Feng J et al. 2007 An x-ray streak camera with high spatio-temporal resolution *Appl. Phys. Lett.* **91** 134102

[14] Shakya M M and Chang Z 2005 Achieving 280 fs resolution with streak camera by reducing deflection dispersion *Appl. Phys. Lett.* **87** 041103

[15] Eckle P et al. 2008 Attosecond Angular Streaking *Nature* **4** 565

[16] Goulielmakis E et al. 2008 Single-Cycle Nonlinear Optics *Science* **320** 1614

[17] Sansone G et al. 2006 Isolated Single-Cycle Attosecond Pulses *Science* **314** 443

[18] Gensch M et al. 2008 New infrared undulator beamline at FLASH *Infr. Phys. Techn.* **51** 423-425

[19] Borisov V, Matushevsky E, Morozov N, Syresin E, Grimm O, Yurkov M, Rossbach J 2006 Simulation of Electromagnetic undulator for far infrared coherent source of TTF at Desy *Proceedings of EPAC 2006* 3595-3597

[20] Frühling, U et al. 2009 Single-shot terahertz-field-driven X-ray streak camera *Nature Phot.* **3** 523-528

[21] Goulielmakis E et al. 2004 Direct Measurement of Light Waves *Science* **305** 1267-1269

[22] Feldhaus J, Grimm O, Kozlov O, Plönjes E, Rossbach J, Saldin E, Scheidmiller E, Yurkov M 2005 The infrared undulator project at the VUV-FEL *Proceedings of the 27th International Free Electron Laser Conference* 183-186

[23] Itatani J, Quéré F, Yudin G L, Ivanov M Yu, Krausz F and Corkum P B 2002 Attosecond Streak Camera *Phys. Rev. Lett.* **88** 173903

[24] Kienberger R et al 2004 Atomic transient recorder *Nature* **427** 817

[25] Glover T E, Schoenlein R W, Chin A H and Shank C V 1996 Observation of Laser Assisted Photoelectric Effect and Femtosecond High Order Harmonic Radiation *Phys. Rev. Lett.* **76** 2468

[26] Gahl C et al 2008 A femtosecond X-ray/optical cross-correlator *Nature Phot.* **2** 165

[27] Cunovic S et al 2007 Time-to-space mapping in a gas medium for the temporal characterization of vacuum-ultraviolet pulses *Appl. Phys. Lett.* **90** 121112

[28] Maltezopoulos Th et al. 2008 Single-shot timing measurement of extreme-ultraviolet free-electron laser pulses *New J. Phys.* **10** 033026

[29] Krikunova M et al. 2009 Time-resolved ion spectrometry on xenon with the jitter-compensated soft x-ray pulses of a free-electron laser *New J. Phys.* **11** 123019

[30] Penet F, Palaudoux J, Lablanquie P and Andric L 2005 Multielectron spectroscopy: The xenon 4d hole double Auger decay *Phys. Rev. Lett.* **95** 083002

[31] Uiberacker M et al 2007 Attosecond real-time observation of electron tunnelling in atoms *Nature Phys.* **446** 627

[32] Jurvansuu M, Kivimäki A and Aksela S 2001 Inherent lifetime widths of Ar $2p^{-1}$, Kr $3d^{-1}$, Xe $3d^{-1}$, and Xe $4d^{-1}$ states *Phys. Rev. A* **64** 012502

[33] Richter M, Amusia M Ya, Bobashev SV, Feigl T, Juranić P N, Martins M, Sorokin AA and Tiedke K 2009 Extreme ultraviolet laser excites atomic giant resonance *Phys. Rev. Lett* **102** 163002

[34] Janauskas V, Partanen L, Kucas S, Karazija R, Huttula M, Aksela S and Aksela H 2003 Auger cascade satellites following $3d$ ionization in xenon *J. Phys. B* **36** 4403

[35] Mitzner R et al 2009 Direct autocorrelation of soft-x-ray free-electron-laser pulses by time-resolved two-photon double ionisation of He *Phys. Rev. A* **80** 025402

[36] Azima A et al 2009 Time-resolved pump-probe experiments beyond the jitter limitations at FLASH *Appl. Phys. Lett.* **94** 144102